Selective Magnetic Resonance Correlation Spectroscopy with In-Phase Multiplets

Sébastien J. F. Vincent, Catherine Zwahlen, and Geoffrey Bodenhausen*

Contribution from the Section de Chimie, Université de Lausanne, Rue de la Barre 2, CH-1005 Lausanne, Switzerland

Received April 28, 1993®

Abstract: New two-dimensional nuclear magnetic resonance (NMR) correlation methods are presented which allow one to obtain selected high-resolution multiplets where all signals have positive pure absorption peak shapes. The multiplets do not suffer from any cancellation effects, and their fine structure consists of a simple superposition of square patterns in two-dimensional frequency domain that can be readily interpreted. The intensities of multiplets obey the same simple binomial rules as those in conventional one-dimensional NMR spectra. The methods rely on a transfer of in-phase magnetization during a doubly selective irradiation period. Complications arising from undesirable coherence-transfer phenomena are eliminated either by removing antiphase terms while leaving the in-phase components unaffected or by a combination of spin-locking of in-phase terms and elimination of antiphase terms.

Introduction

The fine structure of cross-peak multiplets in multi-dimensional NMR spectra contains valuable information about the magnitudes and signs of scalar couplings. Several adverse circumstances may however impede the analysis of such multiplets: poor digital resolution, excessive complexity, accidental overlap, and partial cancellation of peaks with opposite signs. The problem of digital resolution can be solved very effectively by "zooming in" on multiplets with the help of two-dimensional methods such as selective correlation spectroscopy (soft-COSY).[1-4] Complex multiplets can be simplified by partial deconvolution of signals once they have been recorded.[5,6] Overlapping multiplets can be separated by three-dimensional spectroscopy[7,8] or by injection of coherence.[9,10] Unfortunately, the cancellation of peaks with opposite signs often makes the interpretation of multiplets difficult both for the human eye and for pattern recognition algorithms.[11] In nonselective correlation experiments,[12] the cancellation problem can be solved by resorting to total correlation spectroscopy (TOCSY),[13] which leads to in-phase multiplets. Unfortunately, the TOCSY method does not give a simple picture of the coupling network, since the presence of a cross-peak does not necessarily prove the existence of a scalar coupling, and the fine structure of TOCSY cross-peak multiplets is difficult to analyze.

In this paper, we describe a method which allows one to obtain the in-phase structure characteristic of TOCSY spectra combined with the simplicity and increased resolution of soft-COSY multiplets.[14] In our approach, we focus attention on a selected pair of spins A and X, and we do not attempt to investigate the entire network of scalar coupled spins in one single experiment. Coherence is transferred by applying two weak radiofrequency fields (actually the sidebands of an audiomodulated field) at the chemical shifts of two selected spins. This leads to a doubly selective homonuclear Hartmann-Hahn (HOHAHA) transfer.[15] This method has been shown to be very effective in one-dimensional spectroscopy (see Appendix), in particular for the selective measurement of relaxation parameters in complicated spectra,[16,17] and also for selective injection of magnetization to separate accidentally overlapping multiplets in two-dimensional spectroscopy (SPLIT-COSY).[10] This paper describes how the doubly selective Hartmann-Hahn effect can be used for "mixing" coherences in homonuclear two-dimensional spectroscopy, in analogy to heteronuclear experiments.[18-20] Doubly selective mixing in homonuclear systems tends to be much simpler and cleaner than the nonselective methods extensively studied elsewhere.[21-25] This method makes it possible to combine the advantages of in-phase magnetization transfer with the resolution and flexibility of selective experiments.

We have dubbed our novel experiment "*p*ure *i*n-*p*hase *c*orrelation *s*pectroscop*y*" (PICSY). It would be improper to speak of "soft TOCSY", since the coherence-transfer process does not deserve the qualification "total", being normally limited to a selected pair of spins. We should also like to avoid confusion with the "semisoft TOCSY" method described by Kessler *et al.*,[26]

* Abstract published in *Advance ACS Abstracts*, August 15, 1993.

(1) Brüschweiler, R.; Madsen, J. C.; Griesinger, C.; Sørensen, O. W.; Ernst, R. R. *J. Magn. Reson.* **1987**, *73*, 380.
(2) Cavanagh, J.; Waltho, J. P.; Keeler, J. *J. Magn. Reson.* **1987**, *74*, 386.
(3) Emsley, L.; Huber, P.; Bodenhausen, G. *Angew. Chem.* **1990**, *102*, 576; *Angew. Chem., Int. Ed. Engl.* **1990**, *29*, 517.
(4) Emsley, L.; Bodenhausen, G. *J. Am. Chem. Soc.* **1991**, *113*, 3309.
(5) LeParco, J.-M.; McIntyre, L.; Freeman, R. *J. Magn. Reson.* **1992**, *97*, 553.
(6) Huber, P.; Bodenhausen, G. *J. Magn. Reson. Ser. A*, **1993**, *102*, 81.
(7) Friedrich, J.; Davies, S.; Freeman, R. *Mol. Phys.* **1988**, *64*, 691.
(8) Griesinger, C.; Sørensen, O. W.; Ernst, R. R. *J. Magn. Reson.* **1989**, *84*, 14.
(9) Müller, N.; Di Bari, L.; Bodenhausen, G. *J. Magn. Reson.* **1991**, *94*, 73.
(10) Zwahlen, C.; Vincent, S. J. F.; Bodenhausen, G. *Angew. Chem.* **1992**, *104*, 1233; *Angew. Chem., Int. Ed. Engl.* **1992**, *31*, 1248.
(11) Pfändler, P.; Bodenhausen, G.; *J. Magn. Reson.* **1987**, *72*, 475.
(12) Ernst, R. R.; Bodenhausen, G.; Wokaun, A. *Principles of Nuclear Magnetic Resonance in One and Two Dimensions*; Clarendon Press: Oxford, England, 1987.
(13) Braunschweiler, L.; Ernst, R. R. *J. Magn. Reson.* **1983**, *53*, 521.
(14) Vincent, S. J. F.; Zwahlen, C.; Bodenhausen, G. *J. Am. Chem. Soc.* **1992**, *114*, 10989.
(15) Konrat, R.; Burghardt, I.; Bodenhausen, G. *J. Am. Chem. Soc.* **1991**, *113*, 9135.
(16) Boulat, B.; Burghardt, I.; Bodenhausen, G. *J. Am. Chem. Soc.* **1992**, *114*, 10679.
(17) Boulat, B.; Bodenhausen, G. *J. Biomolec. NMR.* **1993**, *3*, 335.
(18) Müller, L.; Ernst, R. R. *Mol. Phys.* **1979**, *38*, 963.
(19) Chingas, G. C.; Garroway, A. N.; Bertrand, R. D.; Moniz, W. B. *J. Chem. Phys.* **1981**, *74*, 127.
(20) Levitt, M. H. *J. Chem. Phys.* **1991**, *94*, 30.
(21) Bax, A.; Davis, D. J. *J. Magn. Reson.* **1985**, *65*, 355.
(22) Chandrakumar, N.; Visalakshi, G. V.; Ramaswamy, D.; Subramanian, S. *J. Magn. Reson.* **1986**, *67*, 307.
(23) Chandrakumar, N.; Subramanian, S. *Modern Techniques in High-Resolution FT-NMR*; Springer Verlag: New York, 1987.
(24) Elbayed, K.; Canet, D. *Mol. Phys.* **1990**, *71*, 979.
(25) Zwahlen, C.; Vincent, S. J. F.; Bodenhausen, G. In *Proceedings of the International School of Physics Enrico Fermi*; Maraviglia, B., Ed.; in press.
(26) Kessler, H.; Anders, U.; Gemmecker, G.; Steuernagel, S. *J. Magn. Reson.* **1989**, *85*, 1.

0002-7863/93/1515-9202$04.00/0

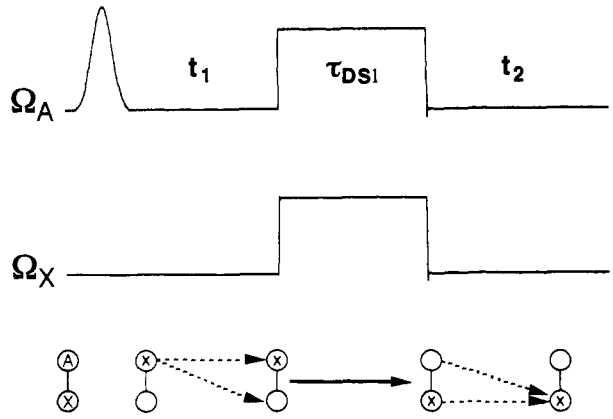

Figure 1. Pulse sequence for the simplest version of pure in-phase spectroscopy ("naive PICSY"). The amplitudes of the two radiofrequency sidebands applied at the chemical shifts Ω_A and Ω_X of two selected spins A and X are shown separately, in analogy to heteronuclear experiments, although the double irradiation is actually achieved by audiomodulation of the radiofrequency carrier placed at $\omega_0 = {}^1/_2(\Omega_A + \Omega_X)$. The product operator evolution graph below[31] shows the most important pathway of magnetization transfer.

where selective excitation of a chosen multiplet is followed by nonselective coherence transfer during a "hard" spin-lock pulse.

Pure In-Phase Correlation Spectroscopy

Figures 1–3 show three alternative methods of increasing sophistication. All three PICSY pulse sequences begin with a selective excitation pulse to excite transverse magnetization of a chosen spin A. This can usually be achieved by a self-refocusing 270° Gaussian pulse.[27] In the "naive" PICSY sequence of Figure 1, the evolution period t_1 is directly followed by a *d*oubly *s*elective *i*rradiation period of duration τ_{DSI} which leads to a transfer of A spin coherence into X spin coherence through a mechanism which will be explained below. The doubly selective irradiation is implemented[28] by placing the carrier frequency midway between the two chemical shifts at $\omega_0 = {}^1/_2(\Omega_A + \Omega_X)$ and by modulating the rectangular pulse envelope with $\cos \omega_a t$, where $\omega_a = {}^1/_2(\Omega_A - \Omega_X)$. This generates two sidebands at frequencies $\omega_0 \pm \omega_a$, which coincide with the chemical shifts of spins A and X. In the improved methods of Figures 2 and 3, the doubly selective irradiation is preceded and followed by other manipulations to suppress undesirable coherence-transfer processes.

In all three PICSY experiments, the free precession Hamiltonian[29] acting on a weakly-coupled two-spin system in the evolution period t_1 is

$$\mathcal{H}^{rot} = \omega_a I_z^A - \omega_a I_z^X + \pi J 2 I_z^A I_z^X \qquad (1)$$

where the chemical shifts are given in a rotating frame synchronized with the carrier at $\omega_0 = {}^1/_2(\omega_0^A + \omega_0^X)$, so that $\Omega_A - \omega_0 = \omega_a$ and $\Omega_X - \omega_0 = -\omega_a$. In a doubly-rotating frame (see below), these chemical shifts formally vanish. The modulation is however reintroduced by using *t*ime-*p*roportional *p*hase *i*ncrements (TPPI), which are required to obtain pure absorption spectra.[12,30] For a two-spin system where the A-spin magnetization is initially excited along the x-axis, we obtain at the end of the evolution period[29]

$$I_x^A \xrightarrow{\mathcal{H}^{rot} t_1} I_x^A \cos \omega_a t_1 \cos \pi J t_1 + 2 I_y^A I_z^X \cos \omega_a t_1 \sin \pi J t_1 + I_y^A \sin \omega_a t_1 \cos \pi J t_1 - 2 I_x^A I_z^X \sin \omega_a t_1 \sin \pi J t_1 \qquad (2)$$

Thus we do not have the simple situation prevailing in one-dimensional doubly selective HOHAHA experiments,[15] where we only have in-phase magnetization I_x^A at the beginning of the τ_{DSI} period (see Appendix). In PICSY sequences, we also have terms I_y^A, $2I_x^A I_z^X$, and $2I_y^A I_z^X$, as well as higher-order terms in systems with more than two spins.[25,29,31] Each of these operator terms will be transformed independently.

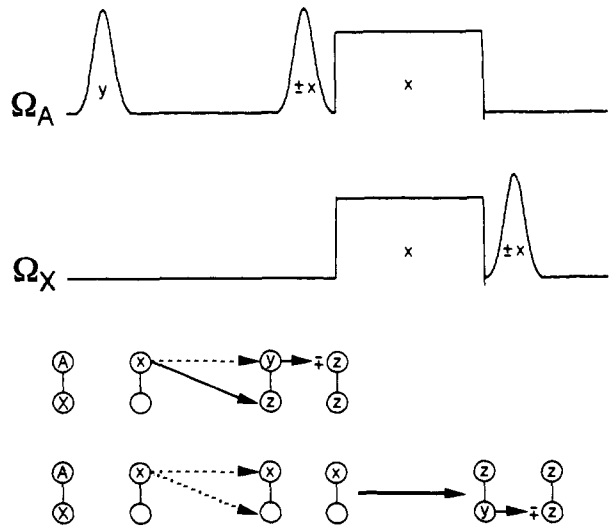

Figure 2. Pulse sequence for "poor man's PICSY" with elimination of undesirable antiphase terms using two self-refocusing 270° Gaussian pulses. The product operator evolution graphs[31] show two perturbing pathways that can be eliminated by the phase-alternation scheme of Table I.

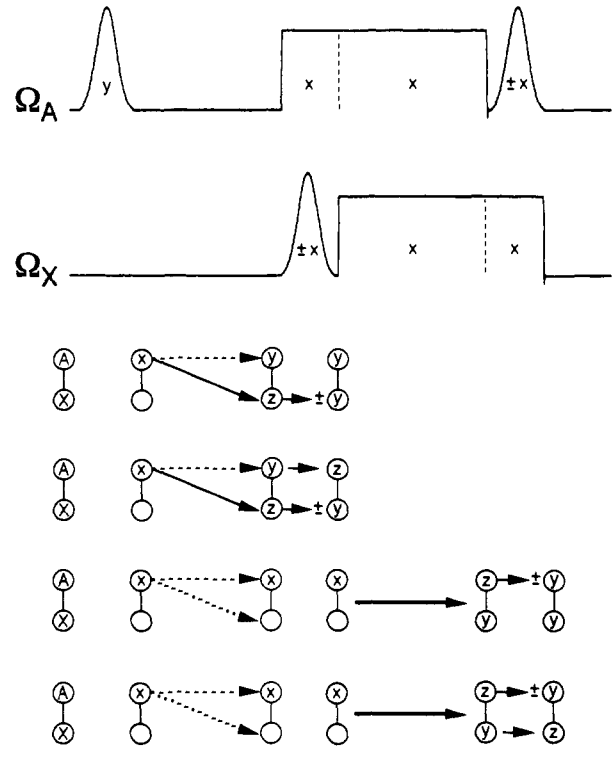

Figure 3. Pulse sequence for "rich man's PICSY" where the desirable in-phase components are locked while the unwanted antiphase terms are eliminated by 270° Gaussian pulses. The product operator evolution graphs[31] show four perturbing pathways that can be eliminated by the phase-alternation scheme of Table I.

Doubly Selective Irradiation

For a two-spin system described in the laboratory frame, the Hamiltonian during the doubly selective irradiation interval τ_{DSI}

(27) Emsley, L.; Bodenhausen, G. *J. Magn. Reson.* **1989**, *82*, 211.
(28) Emsley, L.; Burghardt, I.; Bodenhausen, G. *J. Magn. Reson.* **1990**, *90*, 214; corrigendum *J. Magn. Reson.* **1991**, *94*, 448.
(29) Sørensen, O. W.; Eich, G. W.; Levitt, M. H.; Bodenhausen, G.; Ernst, R. R. *Prog. Nucl. Magn. Reson. Spectrosc.* **1983**, *16*, 163.
(30) Marion, D.; Wüthrich, K. *Biochem. Biophys. Res. Commun.* **1983**, *113*, 967.
(31) Eggenberger, U.; Bodenhausen, G. *Angew. Chem.* **1990**, *102*, 392; *Angew. Chem., Int. Ed. Engl.* **1990**, *29*, 374.

is

$$\mathcal{H}_{DSI}^{lab} = \Omega_A I_z^A + \Omega_X I_z^X + \pi J 2\mathbf{I}^A\cdot\mathbf{I}^X + 2\omega_1 \cos \omega_a t[(I_x^A + I_x^X) \cos \omega_0 t + (I_y^A + I_y^X) \sin \omega_0 t] \quad (3)$$

where $2\omega_1 = -2\gamma B_1$ (expressed in rad s^{-1}) is the total amplitude of the radiofrequency field (ω_1 for each sideband), and J, the scalar coupling constant between A and X. This expression can be transformed into a doubly-rotating (DR) frame,[25,28] also called interaction representation,[32] which is defined so that it rotates at Ω_A for spin A and at Ω_X for spin X:

$$\mathcal{H}_{DSI}^{DR} = \omega_1(I_x^A + I_x^X) + \omega_1(I_x^A \cos 2\omega_a t + I_y^A \sin 2\omega_a t) + \omega_1(I_x^X \cos 2\omega_a t - I_y^X \sin 2\omega_a t) + \pi J 2I_z^A I_z^X + \pi J \cos 2\omega_a t \times (2I_x^A I_x^X + 2I_y^A I_y^X) + \pi J \sin 2\omega_a t\,(2I_x^A I_y^X - 2I_y^A I_x^X) \quad (4)$$

If $\Delta\Omega = 2\omega_a > \omega_1 > \pi J$, the time-dependent parts of this expression can be safely neglected.[25] In practice, we typically have $\Delta\Omega/2\pi > 100$ Hz, 50 Hz $> \omega_1/2\pi >$ 20 Hz, and $J/2 < 10$ Hz. The terms proportional to ω_1 and rotating at $\pm 2\omega_a$ describe the effect on spin A of the sideband located at the chemical shift of spin X and vice versa, which may be regarded as a Bloch–Siegert effect.[25] Thus we obtain the simplified time-independent Hamiltonian

$$\mathcal{H}_{DSI}^{DR} = \omega_1(I_x^A + I_x^X) + \pi J 2I_z^A I_z^X \quad (5)$$

The evolution can be calculated analytically by integrating the equation of motion[12,32]

$$d\sigma(t)/dt = -i[\mathcal{H},\sigma(t)] \quad (6)$$

In this paper, we shall focus attention on terms that may contribute to a signal in the vicinity of spin X. By using a shorthand notation for the frequencies that are relevant in the τ_{DSI} period

$$\omega_J = \pi J \quad (7)$$

$$\omega_{eff} = (4\omega_1^2 + \pi^2 J^2)^{1/2} \quad (8)$$

the first two terms of eq 2 transform as follows:

$$I_x^A \xrightarrow{\mathcal{H}_{DSI}^{DR}\tau_{DSI}} I_x^X\,{}^1/_2[-\cos \omega_J\tau_{DSI} + (\omega_J/\omega_{eff})^2 \cos \omega_{eff}\tau_{DSI} + (2\omega_1/\omega_{eff})^2] + 2I_z^A I_y^X\,{}^1/_2[-\sin \omega_J\tau_{DSI} + (\omega_J/\omega_{eff}) \sin \omega_{eff}\tau_{DSI}] \quad (9)$$

disregarding four irrelevant terms proportional to I_x^A, $2I_y^A I_z^X$, $2I_z^A I_z^X$, and $2I_y^A I_y^X$, and

$$2I_y^A I_z^X \xrightarrow{\mathcal{H}_{DSI}^{DR}\tau_{DSI}} I_x^X\,{}^1/_2[\sin \omega_J\tau_{DSI} - (\omega_J/\omega_{eff}) \sin \omega_{eff}\tau_{DSI}] + 2I_z^A I_y^X\,{}^1/_2[-\cos \omega_J\tau_{DSI} + \cos \omega_{eff}\tau_{DSI}] \quad (10)$$

without including four irrevelant terms proportional to I_x^A, $2I_y^A I_z^X$, $2I_z^A I_z^X$, and $2I_y^A I_y^X$.

Figure 4 shows the transfer functions of eqs 9 and 10. The last two terms of eq 2 transform as follows:

$$I_y^A \xrightarrow{\mathcal{H}_{DSI}^{DR}\tau_{DSI}} 2I_x^A I_y^X[(2\omega_1/\omega_{eff}) \sin {}^1/_2\omega_J\tau_{DSI} \sin {}^1/_2\omega_{eff}\tau_{DSI}] \quad (11)$$

dropping three irrevelant terms proportional to I_y^A, I_z^A, and $2I_x^A I_z^X$, and

$$2I_x^A I_z^X \xrightarrow{\mathcal{H}_{DSI}^{DR}\tau_{DSI}} -2I_x^A I_y^X[(2\omega_1/\omega_{eff}) \cos {}^1/_2\omega_J\tau_{DSI} \sin {}^1/_2\omega_{eff}\tau_{DSI}] \quad (12)$$

disregarding three irrelevant terms proportional to I_y^A, I_z^A, and

(32) Goldman, M. *Quantum Description of High-Resolution NMR in Liquids*; Clarendon Press: Oxford, England, 1988.

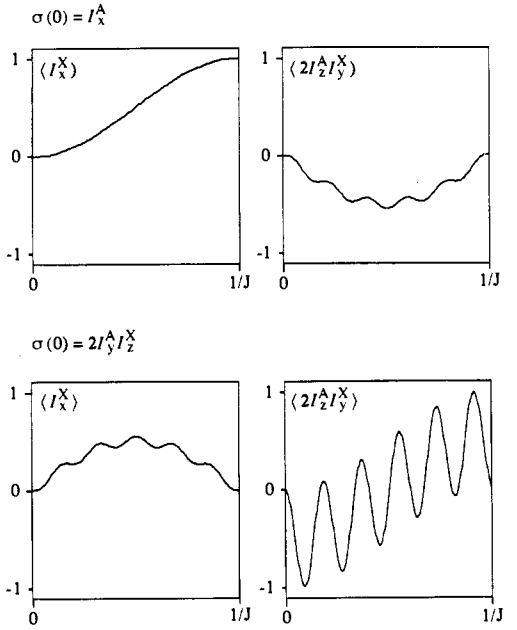

Figure 4. Evolution of a few relevant product operator terms during a doubly selective irradiation of duration $0 < \tau_{DSI} < 1/J$ for initial conditions $\sigma(0) = I_x^A$ (top) and $\sigma(0) = 2I_y^A I_z^X$ (below). The plots correspond to the analytical expressions of eqs 9 and 10, respectively. The parameters used to generate these graphs were similar to experimental conditions, i.e. $J = 5$ Hz and a radiofrequency amplitude $\omega_1/2\pi = 13.7$ Hz. The latter was chosen to illustrate how the coefficient of $2I_z^A I_y^X$ vanishes at $\tau_{DSI} = 1/J$ if eq 25 is fulfilled with $n = 5$.

$2I_x^A I_z^X$. Note that the $2I_z^A I_z^X$, $2I_y^A I_y^X$, and $2I_x^A I_y^X$ terms are not in themselves observable but that they could be converted into signals appearing in the vicinity of the X resonance after further pulses. They must therefore be borne in mind if the doubly selective irradiation period is followed by other manipulations. A phase cycle may be necessary to remove signal contributions arising from these stray terms.

For $2\omega_a \gg \omega_1$, the analytical and numerical calculations based on the full Hamiltonian of eq 3 are virtually undistinguishable. However, if the radiofrequency amplitude ω_1 of each sideband exceeds, say, one-tenth of the chemical shift separation $\Delta\Omega = 2\omega_a$, slight discrepancies make their appearance. Figure 5 shows how the crucial transfer function from I_x^A into I_x^X is affected under these conditions. These simulations clearly show the validity of the assumptions made between eqs 4 and 5, since we usually have $\omega_1/2\omega_a < 0.1$ in our experiments.

Signal Contributions

To obtain pure in-phase multiplets, the magnetization-transfer process that must be selected during the mixing period τ_{DSI} is the conversion of I_x^A into I_x^X, which is sketched in Figure 1 using the conventions of product operator evolution graphs[31] which give a graphical representation of the Cartesian product operator formalism.[12,29] The pairs of circles connected by vertical lines represent the scalar coupled spins A and X; the symbols x, y, and z indicate whether these spins are associated with I_x, I_y, or I_z operators, while empty circles stand for unity operators. Long horizontal arrows represent precession under chemical shifts, while sloping arrows represent transformations under scalar couplings. Short horizontal arrows show transformations due to radiofrequency pulses. Solid arrows indicate transformations associated with sinusoidal coefficients, while dashed arrows depict non-transformations associated with cosinusoidal coefficients. The bold horizontal arrows drawn under the doubly selective irradiation periods in Figures 1–3 symbolize Hartmann-Hahn-transfer processes, which were not anticipated in the work of Eggenberger.[31] It is obvious from eqs 9–12 that many pathways may

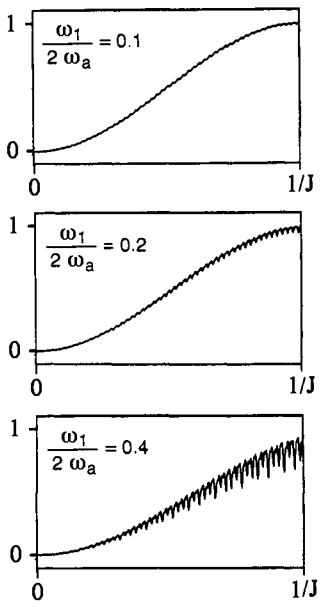

Figure 5. Transfer of the desirable in-phase component I_x^A into I_x^X as a function of $0 < \tau_{DSI} < 1/J$ for various ratios $\omega_1/2\omega_a$, with $J = 5$ Hz throughout. The chemical shift difference and hence the modulation frequency $\omega_a/2\pi = 125$ Hz were kept constant while ω_1 was varied.

give rise to observable X-spin magnetization, some of which lead to dispersive and/or antiphase contributions to the signal. We assume for simplicity (without loss of generality) that the detector picks up the x-component of the magnetization, i.e. that the observed signal is given by $s(t) = \mathrm{Tr}\{I_x\sigma(t)\}$. Consider first the desired pathway, shown in Figure 1:

$$I_x^A \xrightarrow{\mathcal{H}^{rot}t_1} I_x^A \xrightarrow{\mathcal{H}_{DSI}^{DR}\tau_{DSI}} I_x^X \xrightarrow{\mathcal{H}^{rot}t_2} I_x^X \qquad (13)$$

For $J = 5$ Hz and $\omega_1/2\pi = 25$ Hz, we have $(\omega_J/\omega_{eff})^2 \approx 0.01$ and $(2\omega_1/\omega_{eff})^2 \approx 1$ in eq 9. The amplitude of the signal is therefore approximately given by

$$s(t_1,\tau_{DSI},t_2) = {}^1/_2 \cos\omega_a t_1 \cos\pi J t_1 \times (1 - \cos\omega_J\tau_{DSI}) \cos\omega_a t_2 \cos\pi J t_2 \quad (14)$$

If the carrier is positioned at $\omega_0 = {}^1/_2(\Omega_A - \Omega_X)$ throughout, as implied in eq 14, the multiplet would be centered at ω_a in both ω_1 and ω_2 dimensions. If the carrier is made to jump from Ω_A in t_1 to Ω_X in t_2, these offsets vanish. After two-dimensional Fourier transformation and phase correction, this gives rise to a pure in-phase doublet in both frequency dimensions[12] with an amplitude given by ${}^1/_2(1 - \cos\omega_J\tau_{DSI})$. The maximum transfer of in-phase coherence from I_x^A into I_x^X is to a very good approximation obtained when $\cos\omega_J\tau_{DSI} = -1$, which gives the "matching condition"

$$\tau_{DSI} = 1/J \qquad (15)$$

We must also consider the following pathway (see Figures 2 and 3):

$$I_x^A \xrightarrow{\mathcal{H}^{rot}t_1} I_x^A \xrightarrow{\mathcal{H}_{DSI}^{DR}\tau_{DSI}} 2I_z^A I_y^X \xrightarrow{\mathcal{H}^{rot}t_2} I_x^X \qquad (16)$$

We may again simplify eq 9 if $J = 5$ Hz and $\omega_1/2\pi = 25$ Hz. Thus the amplitude of the signal due to this process is approximately

$$s(t_1,\tau_{DSI},t_2) = -{}^1/_2 \cos\omega_a t_1 \cos\pi J t_1 \sin\omega_J\tau_{DSI} \cos\omega_a t_2 \sin\pi J t_2 \quad (17)$$

With the same phase correction as before, this yields an absorptive in-phase doublet in ω_1 and a dispersive antiphase doublet in ω_2 with an amplitude given by $-{}^1/_2 \sin\omega_J\tau_{DSI}$.

Now consider the pathway

$$I_x^A \xrightarrow{\mathcal{H}^{rot}t_1} 2I_y^A I_z^X \xrightarrow{\mathcal{H}_{DSI}^{DR}\tau_{DSI}} 2I_z^A I_y^X \xrightarrow{\mathcal{H}^{rot}t_2} I_x^X \qquad (18)$$

The resulting contribution to the signal amplitude is (see eq 10)

$$s(t_1,\tau_{DSI},t_2) = {}^1/_2 \cos\omega_a t_1 \sin\pi J t_1(\cos\omega_J\tau_{DSI} - \cos\omega_{eff}\tau_{DSI}) \cos\omega_a t_2 \sin\pi J t_2 \quad (19)$$

If we use again the same phase correction, this gives rise to a dispersive antiphase doublet in both frequency domains with an amplitude ${}^1/_2(\cos\omega_J\tau_{DSI} - \cos\omega_{eff}\tau_{DSI})$.

Finally, we must consider the pathway

$$I_x^A \xrightarrow{\mathcal{H}^{rot}t_1} 2I_y^A I_z^X \xrightarrow{\mathcal{H}_{DSI}^{DR}\tau_{DSI}} I_x^X \xrightarrow{\mathcal{H}^{rot}t_2} I_x^X \qquad (20)$$

If we neglect the term proportional to (ω_J/ω_{eff}) in eq 10, the amplitude of the signal due to this pathway is

$$s(t_1,\tau_{DSI},t_2) = {}^1/_2 \cos\omega_a t_1 \sin\pi J t_1 \sin\omega_J\tau_{DSI} \cos\omega_a t_2 \cos\pi J t_2 \quad (21)$$

which gives rise to a dispersive antiphase doublet in ω_1 and an absorptive in-phase doublet in ω_2 with an amplitude ${}^1/_2 \sin\omega_J\tau_{DSI}$.

In the "matched" case where $\tau_{DSI} = 1/J$ (eq 15), the pathways involving a conversion, $I_x^A \rightarrow 2I_z^A I_y^X$ (eq 17) and $2I_y^A I_z^X \rightarrow I_x^X$ (eq 21), can be neglected. Indeed, as shown in Figure 4, the expectation values of $2I_z^A I_y^X$ (Figure 4, top right) and I_x^X (Figure 4, bottom left) due to these transfers vanish at the end of the doubly selective irradiation period. But the conversion of $2I_y^A I_z^X$ into $2I_z^A I_y^X$ of eq 19 may present a problem even if $\tau_{DSI} = 1/J$. The transfer function shown in Figure 4 (bottom right) oscillates rapidly with ω_{eff} (see eq 10) and vanishes if and only if

$$\cos\omega_{eff}\tau_{DSI} = \cos\omega_J\tau_{DSI} \qquad (22)$$

In the case where the condition $\tau_{DSI} = 1/J$ for optimum transfer is fulfilled, we obtain with the definitions of eqs 7 and 8

$$\cos[(4\omega_1^2 + \pi^2J^2)^{1/2}/J] = \cos\pi = -1 \qquad (23)$$

hence

$$(4\omega_1^2 + \pi^2J^2)^{1/2} = \pi J(2n + 1) \qquad (24)$$

with $n = 0, 1, 2, \ldots$. This gives a condition for the radiofrequency amplitude $\nu_1 = \omega_1/2\pi$ (expressed in Hz) of each sideband

$$\nu_1 = {}^1/_2 J[n(n + 1)]^{1/2} \qquad (25)$$

The integer $n = 0, 1, 2, \ldots$ may be chosen so that the radiofrequency amplitude is typically in the range $10 < \nu_1 < 40$ Hz, so that spin-locking is efficient for all components within a multiplet, without risking to perturb other spins too much. In Figure 4, we have chosen a radiofrequency amplitude $\nu_1 = 13.7$ Hz corresponding to $n = 5$ and $J = 5$ Hz. It is apparent that the expectation value $2I_z^A I_y^X$ vanishes at the end of $\tau_{DSI} = 1/J$ as predicted. Unfortunately, the prescription of eq 25 is not very convenient to fulfill in practice, for the precise value of J is unlikely to be known, and it may be difficult to adjust the radiofrequency amplitude with sufficient accuracy. Furthermore, transverse relaxation may imply that the optimum of the in-phase transfer occurs for $\tau_{DSI} < 1/J$. Thus we should develop alternative strategies for the suppression of unwanted signals that do not require adapting the duration τ_{DSI} and the radiofrequency amplitude ω_1 to the magnitude of the scalar coupling.

Poor Man's PICSY

This is where we shall ask our pixie to fulfill our wishes. In the pulse sequence of Figure 2, the undesirable terms are removed

Table I. Phase Alternation of the Three 270° Pulses in Either PICSY Sequence of Figure 2 or 3

scan number	excitation	1st purge	2nd purge	receiver
1	y	x	x	+
2	$-y$	x	x	−
3	y	$-x$	x	+
4	$-y$	$-x$	x	−
5	y	x	$-x$	+
6	$-y$	x	$-x$	−
7	y	$-x$	$-x$	+
8	$-y$	$-x$	$-x$	−

by 270° Gaussian pulses before and after the HOHAHA transfer. These purging pulses are applied along the $\pm x$-axes, i.e. parallel to the desirable in-phase terms I_x^A and I_x^X in order to lock these in-phase components. The first 270° pulse applied at Ω_A also transforms the unwanted antiphase term (see previous section) into longitudinal two-spin order with an alternating sign:

$$2I_y^A I_z^X \xrightarrow{270°_{\pm x}(\Omega_A)} \mp 2I_z^A I_z^X \tag{26}$$

This cannot lead to any signal contributions if the transients are added (see Table I). The I_y^A term present at the end of the evolution period (eq 2) is transformed into longitudinal magnetization, again with an alternating sign:

$$I_y^A \xrightarrow{270°_{\pm x}(\Omega_A)} \mp I_z^A \tag{27}$$

The $2I_x^A I_z^X$ term remains invariant, but this cannot give rise to any observable coherence on spin X after doubly selective irradiation (see eq 12).

At the end of the doubly selective irradiation interval, a second 270°$_{\pm x}$ Gaussian pulse is applied at Ω_X (Figure 2) to eliminate the antiphase term $2I_z^A I_y^X$

$$2I_z^A I_y^X \xrightarrow{270°_{\pm x}(\Omega_X)} \mp 2I_z^A I_z^X \tag{28}$$

which cannot give rise to any signals. The term I_x^X remains invariant. The purging pulse converts the $2I_z^A I_z^X$ term into $\pm 2I_z^A I_y^X$; this is eliminated by adding the signals as in Table I. It is most convenient to ensure phase coherence between the last pulse and the doubly selective irradiation if the latter's duration is a multiple of the period of the modulation frequency:

$$\tau_{DSI} = 2n\pi/\omega_a \tag{29}$$

where $n = 1, 2, 3, \ldots$.

Rich Man's PICSY

In the most elaborate PICSY sequence shown in Figure 3, the desirable in-phase component I_x^A is locked by a radiofrequency field component applied at Ω_A while at 270° Gaussian pulse is applied at Ω_X along the $\pm x$-axes (see Table I). This removes the $2I_y^A I_z^X$ term which arises at the end of the evolution period (see eqs 2 and 21):

$$2I_y^A I_z^X \xrightarrow{\text{lock}_x(\Omega_A) + 270°_{\pm x}(\Omega_X)} \pm 2I_y^A I_y^X \cos\beta \pm 2I_z^A I_y^X \sin\beta \tag{30}$$

where the angle β represents the angle of nutation of magnetization components that are orthogonal to the axis of the spin-locking field, $\beta = \omega_1 \tau_{270°}$, ω_1 being the amplitude of the spin-locking field and $\tau_{270°}$ the duration of the 270° pulse, which corresponds to the initial part of the spin-locking interval, up to the first vertical dashed line of Figure 3. The desirable in-phase term I_x^A is neatly locked by the selective field applied at Ω_A and remains invariant.

The 270°$_{\pm x}(\Omega_X)$ pulse before the doubly selective irradiation period introduces a new term by transforming the equilibrium magnetization I_z^X into $\pm I_y^X$. Fortunately, all "offspring" of this term is eliminated by phase alternation. The last two product operator terms involved in eq 2 are also transformed: I_y^A into $I_y^A \cos\beta + I_z^A \sin\beta$ and $2I_x^A I_z^X$ into $\pm 2I_x^A I_y^X$. The latter term is again eliminated by phase cycling, while I_y^A and I_z^A cannot give rise to signals in the X-spin region.

After the doubly selective irradiation, the last 270°$_{\pm x}(\Omega_A)$ pulse (Figure 3) converts the $2I_z^A I_y^X$ term (which stems from I_x^A, see eqs 9 and 17) into bilinear terms that do not contribute to the X-spin signal:

$$2I_z^A I_y^X \xrightarrow{270°_{\pm x}(\Omega_A) + \text{lock}_x(\Omega_X)} \pm 2I_y^A I_y^X \cos\beta \pm 2I_y^A I_z^X \sin\beta \tag{31}$$

At the same time, the desirable I_x^X term is spin-locked so that it cannot evolve further under the effect of scalar couplings. Provided the last 270° pulse is applied exactly along the $\pm x$-axes, the $2I_x^A I_y^X$ term appearing at the end of the doubly selective irradiation (eqs 11 and 12) cannot be transformed into observable coherence on spin X:

$$2I_x^A I_y^X \xrightarrow{270°_{\pm x}(\Omega_A) + \text{lock}_x(\Omega_X)} 2I_x^A I_y^X \cos\beta + 2I_x^A I_z^X \sin\beta \tag{32}$$

Thus it is again essential to have a definite phase relationship between the 270° Gaussians and the radiofrequency sidebands during the doubly selective irradiation interval; otherwise the transformation of eq 32 would be jeopardized. It is also important that the magnetization remains locked throughout the spin-locking periods, without interruption at the vertical dashed lines drawn in Figure 3.

In the case where τ_{DSI} is equal to the matched value of $1/J$ (eq 15), one of the purging pulses in Figure 2 or 3 can be dropped, since the pathways $I_x^A \rightarrow 2I_z^A I_y^X$ (eq 17) and $2I_y^A I_z^X \rightarrow I_x^X$ (eq 21) can be neglected. Nevertheless, the transfer of $2I_y^A I_z^X \rightarrow 2I_z^A I_y^X$ (eq 19) still represents a problem, so that it must be eliminated either before or after the doubly selective irradiation period.[14]

Comparison of Methods

The naive PICSY method of Figure 1 can only be applied if the value of the active coupling constant is known before setting up the experiment, so that one can choose (i) the doubly selective irradiation period according to eq 15 and (ii) the radiofrequency amplitude according to eq 25. This is not very convenient in practice, although reasonable spectra have been obtained (see Figure 6b).

Although both PICSY methods of Figures 2 and 3 suppress undesirable signal contributions by phase alternation, there are some significant differences. In poor man's PICSY (Figure 2), one merely needs to shift the carrier frequency twice and to use either monochromatic or amplitude-modulated pulses, whereas, in rich man's PICSY (Figure 3), it is necessary to superimpose phase-modulated pulses. A second and more subtle difference lies in the properties of the purging pulses. In poor man's PICSY, these pulses must be self-refocusing, because a pulse which would fail to convert transverse coherence into longitudinal magnetization would lead to unwanted signals, despite the phase alternation. Thus in contrast to the case of eq 28, one would be left with some $2I_z^A I_y^X$ at the beginning of the detection period. In rich man's PICSY, the unwanted $2I_z^A I_y^X$ component at the end of the doubly selective irradiation (eq 31) will be completely eliminated, provided the purging pulse transforms longitudinal magnetization I_z^A into transverse coherence I_x^A *or* I_y^A. Thus the purging pulse need not have any self-refocusing properties. This clearly gives additional degrees of freedom in the design of the PICSY method of Figure 3.

Finally, the decisive argument in favor of rich man's PICSY is that the rectangular pulse is more efficient in locking the

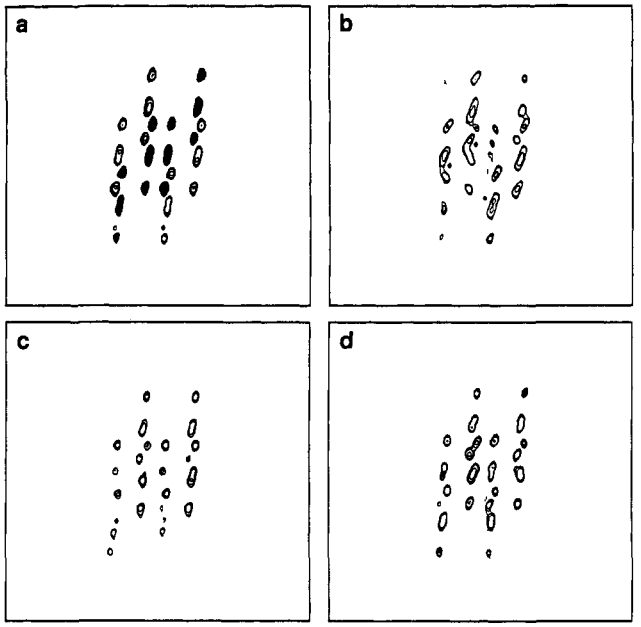

Figure 6. Multiplets correlating the β^{cis} proton (centered at 1.23 ppm in the vertical ω_1 domain) and the β^{trans} proton (at 2.79 ppm in the horizontal ω_2 domain) of D-proline[3] (I) in cyclo(L-Pro[1]-L-Pro[2]-D-Pro[3]) at 303 K: (a) soft-COSY (negative peaks are filled in black); (b) naive PICSY of Figure 1 with a duration $\tau_{DSI} = 84.0$ ms $\simeq 1/J_{\beta^{cis}\beta^{trans}}$; (c) Poor man's PICSY of Figure 2 with a duration of $\tau_{DSI} = 63.9$ ms $= 15 \times 2\pi/\omega_a \neq 1/J_{\beta^{cis}\beta^{trans}}$, using the phase cycle of Table I; (d) rich man's PICSY of Figure 3 with the same duration and phase cycle. All 270° Gaussian pulses were 30 ms long. For each t_1-increment, 8 scans were recorded; the spectral widths were 75 Hz in ω_1 and 1500 Hz in ω_2 in all cases (only 75 × 75 Hz are shown). The matrices consisted of 128 × 8K data points before and 256 × 8K data points after zero filling. Lorentz–Gauss transformations (LB = –0.3, GB = 0.05 in ω_1 and LB = –0.1, GB = 0.05 in ω_2) were applied in both dimensions before Fourier transformation.

desirable in-phase magnetization than the 270° pulse in poor man's PICSY. This can be shown experimentally by applying a 270°$_y$ Gaussian pulse to an isolated multiplet, followed either by a 270°$_x$ Gaussian pulse or by a rectangular pulse along the x-axis. The second experiment (which mimics the locking of in-phase magnetization in rich man's PICSY) gives a more intense multiplet than the first experiment (which simulates the purging used in poor man's PICSY). In addition, one should consider the influence of couplings to passive spins which lead to wider multiplets and introduce effects that are similar to offsets. The simultaneous irradiation of both spins in the case of rich man's PICSY reduces this problem by effectively reducing the width of the multiplet.

Examples

Figure 6a shows a soft-COSY spectrum correlating the β^{cis} and β^{trans} protons of the D-proline[3] residue of cyclo(L-Pro[1]-L-Pro[2]-D-Pro[3]).[33] The spin system of this amino acid can be represented by a graph illustrating the coupling network in which the nodes represent the spins and the edges their mutual couplings (I).[34,35] This is compared with three PICSY spectra of increasing sophistication (pulse sequences of Figures 1–3) of the same multiplet. The initial self-refocusing 270° Gaussian pulse[27] is applied in the vicinity of the chemical shift of the β^{cis} proton. One typically needs a duration of 30 ms for a multiplet of 30 Hz width; a multiplet of 50 Hz across requires harder pulses of about 18-ms duration. If the phase dispersion induced by the 270° Gaussian pulse is too large, one can use more sophisticated pulses

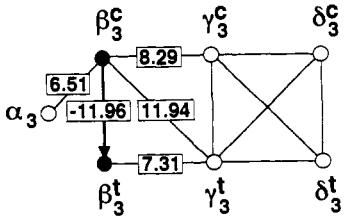

I

such as Gaussian cascades optimized by quaternions[36] or E-BURP pulses.[37,38] The doubly selective irradiation is generated by placing the radiofrequency carrier at $\omega_0 = {}^1/_2(\Omega_{\beta^{cis}} + \Omega_{\beta^{trans}})$ (2.01 ppm) while the amplitude is modulated with cos $\omega_a t$, where $\omega_a = {}^1/_2(\Omega_{\beta^{cis}} - \Omega_{\beta^{trans}})$ (234.5 Hz). The naive PICSY spectrum of Figure 6b has been acquired with $\tau_{DSI} = 84.0$ ms $\simeq 1/J_{\beta^{cis}\beta^{trans}} = 1/12.0$[33,34] according to eq 15; the radiofrequency amplitude was adjusted close to the condition of eq 25 with $n = 4$. In the poor man's PICSY (Figure 6c), all purging pulses were 270° Gaussians of 30 ms and τ_{DSI} was set to $15(2\pi/\omega_a) = 63.9$ ms (see eq 29). Note that one does *not* need to know the value of the active coupling constant J in order to set this condition. The phases were cycled according to Table I. In rich man's PICSY (Figure 6d), the purging pulses were achieved by superposition of two phase-modulated wave forms, one with an amplitude shaped as a 270° Gaussian and an effective frequency $\omega_0 \pm \omega_a$, the other with a constant amplitude ω_1 and an effective frequency $\omega_0 \mp \omega_a$. The 270° Gaussian pulses used for purging are identical to those used at the beginning of the sequences for selective excitation. We used again $\tau_{DSI} = 63.9$ ms as in Figure 6c. The phases were in this case cycled according to Table I. In all four spectra, *t*ime-*p*roportional *p*hase *i*ncrements (TPPI)[12,30] are applied to the initial excitation pulse. The wave forms were generated by an Oxford Research Systems selective excitation unit used in conjunction with a Bruker MSL 300 spectrometer.

The naive PICSY spectrum in Figure 6b appears contaminated by antiphase signal contributions, as evidenced by ugly line shapes and small negative peaks (filled in black). The poor man's PICSY spectrum in Figure 6c shows nice peak shapes without negative signal contributions, but the intensity of the peaks appears attenuated near the edges of the multiplet. In the rich man's PICSY spectrum of Figure 6d, these intensity problems have vanished. To acquire the latter two spectra, the duration of the doubly selective irradiation was deliberately shortened to demonstrate that the matching condition of eq 15 need not be fulfilled. The efficiency of the transfer was therefore reduced according to eq 14. No effort was made to adjust the radiofrequency amplitude to the condition of eq 25.

Figure 7 shows a comparison of two PICSY spectra correlating the β^{cis} and α protons of the L-proline[2] residue of cyclo(L-Pro[1]-L-Pro[2]-D-Pro[3])[33] obtained with the two methods of Figures 2 and 3. The multiplets show four passive couplings in accordance with the coupling network of this proline (II).[33]

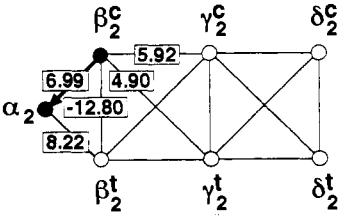

II

Both spectra in Figure 7 were obtained with a doubly selective irradiation period that was much shorter than the matched condition $\tau_{DSI} = 1/J$. The corresponding sections of Figure 8 clearly show the superiority of rich man's PICSY in preserving

(33) Kessler, H.; Bermel, W.; Friedrich, A.; Krack, G.; Hull, W. E. *J. Am. Chem. Soc.* **1982**, *104*, 6297.
(34) Novič, M.; Bodenhausen, G. *Anal. Chem.* **1988**, *60*, 582.
(35) Pfändler, P.; Bodenhausen, G. *J. Magn. Reson.* **1988**, *79*, 99.
(36) Emsley, L.; Bodenhausen, G. *J. Magn. Reson.* **1992**, *97*, 135.
(37) Geen, H.; Wimperis, S.; Freeman, R. *J. Magn. Reson.* **1989**, *85*, 620.
(38) Geen, H.; Freeman, R. *J. Magn. Reson.* **1991**, *93*, 93.

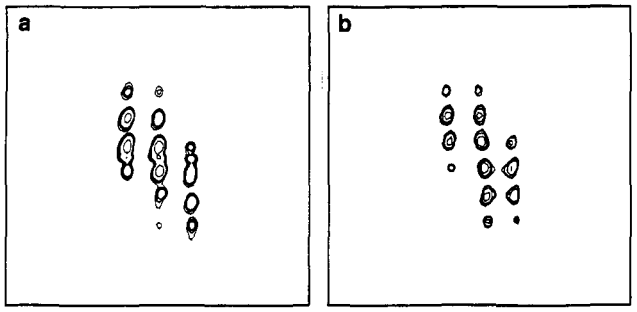

Figure 7. Multiplets correlating the β^{cis} proton (centered at 2.10 ppm in the vertical ω_1 domain) and the α proton (at 4.32 ppm in the horizontal ω_2 domain) of L-Proline[2] (**II**) in cyclo(L-Pro[1]-L-Pro[2]-D-Pro[3]) at 303 K: (a) poor man's PICSY of Figure 2 with a duration of τ_{DSI} = 108.3 ms = $39 \times 2\pi/\omega_a$, shorter than the matched condition $\tau_{DSI} = 1/J_{\alpha\beta^{cis}}$ = 143.1 ms; (b) rich man's PICSY of Figure 3 with the same duration τ_{DSI} = 108.3 ms. Because of the width of the β^{cis} multiplet in the vertical ω_1 domain, the lengths of all 270° Gaussian pulses were reduced to 20 ms. All other conditions were as in Figure 6.

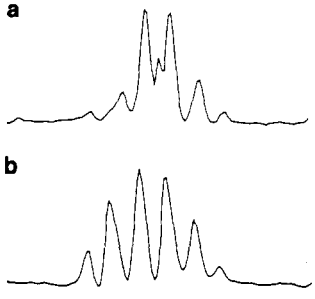

Figure 8. Vertical cross sections through the central columns of the two PICSY spectra of Figure 7: (a) recorded with the PICSY sequence of Figure 2; (b) obtained with the sequence of Figure 3.

the multiplet structure without intensity problems at the edges of the multiplet.

Figure 9 shows a comparison of soft-COSY and rich man's PICSY multiplets correlating the γ^{cis} and δ^{cis} protons of the D-proline[3] residue of cyclo(L-Pro[1]-L-Pro[2]-D-Pro[3]).[33] For both spectra on the top of the figure, all 270° Gaussian pulses had a duration of 30 ms. In the PICSY, the duration of the doubly selective irradiation was set to be τ_{DSI} = 75.4 ms, according to eq 29 with n = 27. The soft-COSY simulation in Figure 9c shows extensive cancellation effects which are due to near-degeneracies among the coupling constants in the coupling network:[33]

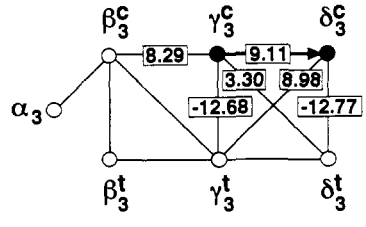

III

Because of the in-phase multiplet structure in PICSY, these disturbing artifacts completely disappear in the experimental PICSY spectra of Figure 9b, so that one can recognize all basic square patterns as shown in the simulation of Figure 9d.

Finally, Figure 10 shows a comparison of soft-COSY and PICSY multiplets correlating the α and β protons of cysteine 30 in *b*asic *p*ancreatic *t*rypsin *i*nhibitor (BPTI).[39] In soft-COSY, all three 270° Gaussian pulses had a duration of 30 ms, whereas, for the PICSY, the first 270° Gaussian also lasted 30 ms, while the 270° Gaussians used for purging had a duration of only 15 ms to reduce relaxation problems. The duration of the doubly

(39) Wagner, G.; Wüthrich, K. *J. Mol. Biol.* **1982**, *155*, 347.

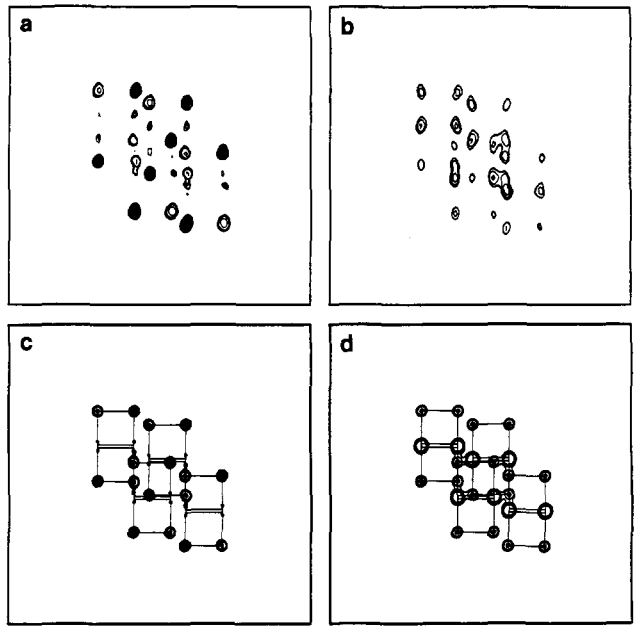

Figure 9. Multiplet correlating the γ^{cis} proton (centered at 1.41 ppm in the vertical ω_1 domain) and the δ^{cis} proton (at 3.81 ppm in the horizontal ω_2 domain) of D-proline[3] (**III**) in cyclo(L-Pro[1]-L-Pro[2]-D-Pro[3]) at 303 K: (a) soft-COSY; (b) rich man's PICSY of Figure 3 with a duration τ_{DSI} = 75.4 ms = $27 \times 2\pi/\omega_a$, much shorter than the matching condition $\tau_{DSI} = 1/J_{\gamma^{cis}\delta^{cis}}$ = 109.7 ms. All other conditions were as in Figure 6. Parts c and d are simulations corresponding to parts a and b, respectively, with the coupling constants given in ref 33 and in Scheme III.

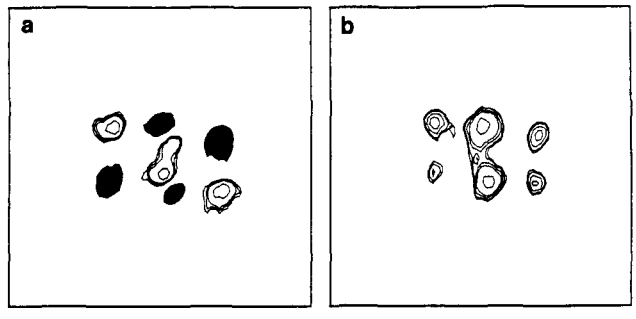

Figure 10. (a) Soft-COSY correlating the α proton (centered at 5.58 ppm in the vertical ω_1 domain) and the β proton (at 3.63 ppm in the horizontal ω_2 domain) of cysteine 30 in basic pancreatic trypsin inhibitor (BPTI)[39] at 327 K. (b) PICSY of Figure 3 with a duration τ_{DSI} = 82.3 ms = $24 \times 2\pi/\omega_a$ using the phase cycle of Table I. The initial 270° Gaussian pulse had a duration of 30 ms; the 270° Gaussian pulses used for purging were shortened to 15 ms to reduce signal losses due to relaxation. For each t_1-increment, 64 scans were acquired; the spectral widths were 75 Hz in ω_1 and 1000 Hz in ω_2 (only 75 × 75 Hz are shown). The matrices consisted of 128 × 2K data points before and 256 × 2K data points after zero filling. A Lorentz-Gauss transformation (LB = −1.0, GB = 0.05) was applied in both dimensions before Fourier transformation. Negative peaks are filled in black.

selective irradiation was set to be τ_{DSI} = 82.3 ms (eq 29 with n = 12). This comparison shows that our methods can also be applied to macromolecules.

Conclusions

We have shown that it is possible to obtain high-resolution pure absorption in-phase multiplets revealing not only scalar couplings between two selected spins A and X but also the couplings to their passive coupling partners. With suitable pulse techniques, one can obtain pure absorption-mode peak shapes in both frequency domains without prior knowledge of the relevant coupling constants. The resulting multiplets do not suffer from any cancellation effects, and their fine structure consists of a

simple superposition of square patterns in two-dimensional frequency domain that can be readily interpreted. The intensities of multiplets obey the same simple binomial rules as those in conventional one-dimensional NMR spectra. The projections of the two-dimensional multiplets on either frequency axis yield multiplets that are identical to those expected in one-dimensional spectra. In this sense, our procedures allow one to unravel overlapping signals.

Acknowledgment. This research was supported by the Fonds National Suisse de la Recherche Scientifique (FNRS) and by the Commission pour l'Encouragement de la Recherche Scientifique (CERS). We gratefully acknowledge a sample of cyclo(L-Pro-L-Pro-D-Pro) from Dr. W. Bermel, Karlsruhe, and Prof. H. Kessler, Garching, a sample of BPTI from Prof. N. Müller, Linz, and the use of simulation programs developed by Dr. L. Emsley.

Appendix: Doubly Selective One-Dimensional HOHAHA

If the evolution period of PICSY experiments vanishes ($t_1 = 0$) and if no purging is used, the initial condition at the beginning of the doubly selective irradiation period consists of pure in-phase magnetization I_x^A, provided we ignore relaxation during the excitation pulse and the phase dispersion resulting from the relatively poor self-refocusing properties of the 270° Gaussian pulse. In this case, we only require the expression given in eq 4 of ref 15 for the one-dimensional doubly selective HOHAHA experiment:

$$\langle I_x^X\rangle(t) = {}^1/_2[(\cos\alpha + \sin\alpha)^2(\cos\alpha - \sin\alpha)^2 + \sin^2 2\alpha\cos((2\omega_1\cos 2\alpha - \pi J\sin 2\alpha)t) - \cos\pi Jt] \quad \text{(A1)}$$

$$\langle 2I_z^A I_y^X\rangle(t) = {}^1/_2[\sin 2\alpha\sin((2\omega_1\cos 2\alpha - \pi J\sin 2\alpha)t) + \sin\pi Jt] \quad \text{(A2)}$$

with $\alpha = {}^1/_2\arctan(-\pi J/2\omega_1)$. If we take the corresponding expectation values from eq 9 of this work, we obtain

$$\langle I_x^X\rangle(t) = {}^1/_2[-\cos\omega_J\tau_{DSI} + (\omega_J/\omega_{eff})^2\cos\omega_{eff}\tau_{DSI} + (2\omega_1/\omega_{eff})^2] \quad \text{(A3)}$$

$$\langle 2I_z^A I_y^X\rangle(t) = {}^1/_2[-\sin\omega_J\tau_{DSI} + (\omega_J/\omega_{eff})\sin\omega_{eff}\tau_{DSI}] \quad \text{(A4)}$$

Except for a change of the sign of the antiphase term, eqs A1 and A3 and eqs A2 and A4 are pairwise identical, as can be shown by using various trigonometric relations. Thus the one-dimensional doubly selective HOHAHA experiment can be considered as a special case of the two-dimensional PICSY method.